JOURNAL OF SOLID STATE CHEMISTRY 94, 89–105 (1991)

An Electron, and X-Ray Powder, Diffraction Study of Cubic, Fluorite-Related Phases in Various ZrO_2–Ln_2O_3 Systems

R. L. WITHERS,* J. G. THOMPSON, AND P. J. BARLOW

Research School of Chemistry, Australian National University, GPO Box 4, Canberra, A.C.T., 2601, Australia

Received January 2, 1991; in revised form April 29, 1991

A detailed electron, and X-ray powder, diffraction study has been made of the cubic, fluorite-related solid solution fields in a range of ZrO_2–Ln_2O_3 systems. A rich variety of composition-dependent diffraction effects were observed, leading to the realization that it is possible for there to be a much more gradual transition between apparently distinct structural types as a function of composition than was previously thought to be the case. Labels such as F-type (or C_1), C-type (or C_2) or pyrochlore as traditionally used are rather inappropriate and unhelpful when attempting to describe structural variations across and between such solid solution fields.

1. Introduction

The structure of pure zirconia, ZrO_2, is reported as being monoclinic from room temperature up to ~1170°C, tetragonal between ~1170°C and ~2370°C, and cubic (fluorite type) from ~2370°C up to the melting point at ~2830°C. Both the monoclinic and the tetragonal forms can be described as displacively modulated variants (albeit with rather substantial displacive modulation amplitudes and, in the case of the tetragonal polymorph, rather substantial isotropic B parameters (*1*)) of the high temperature fluorite-type structure (*2, 3*).

The "stabilization" of the higher temperature polymorphs of ZrO_2 via the addition of a relatively small amount (~5–20 mole%) of the oxides of a variety of lower valent metals—such as CaO, MgO, or the lanthanide sesquioxides Ln_2O_3—and subsequent quenching from sufficiently elevated temperatures (~1600°C) leads to anion-deficient materials with important ceramic and superionic conduction properties. Such properties are strongly dependent upon the extent of compositional modulation (in the form of the distribution of the metal atoms and the oxygen vacancy ordering) and subsequent associated structural relaxation or displacive modulation (*4, 5*). Given that the oxygen array is certainly very mobile at temperatures >1000°C, it is clear that the ordering in the quenched materials is strongly dependent upon the high temperature ordering of the much more rigid metal atom array.

Information as to the type and extent of such compositional and displacive modulation is most directly present in the form of the weak satellite reflections and/or weak diffuse intensity distributions which almost invariably accompany the strong, sharp, Bragg reflections of the underlying fluorite-type average structure. Numerous workers

* To whom correspondence should be addressed.

0022-4596/91 $3.00

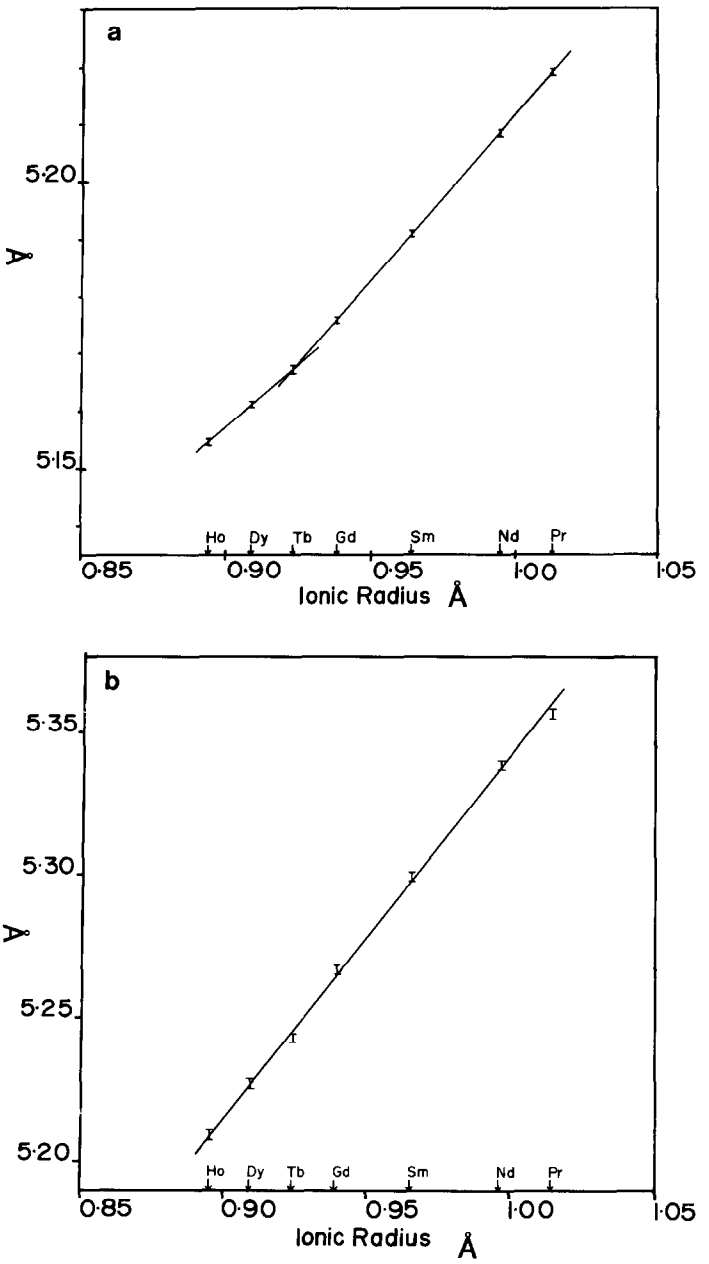

FIG. 1. Refined unit cell dimensions as a function of ionic radius for (a) the 25 mole% (b) the 50 mole% and (c) the 65 mole% $LnO_{1.5}$ specimens. The weighted average cubic cell edges were used in two phase regions. In the pyrochlore region half the cell edge was used.

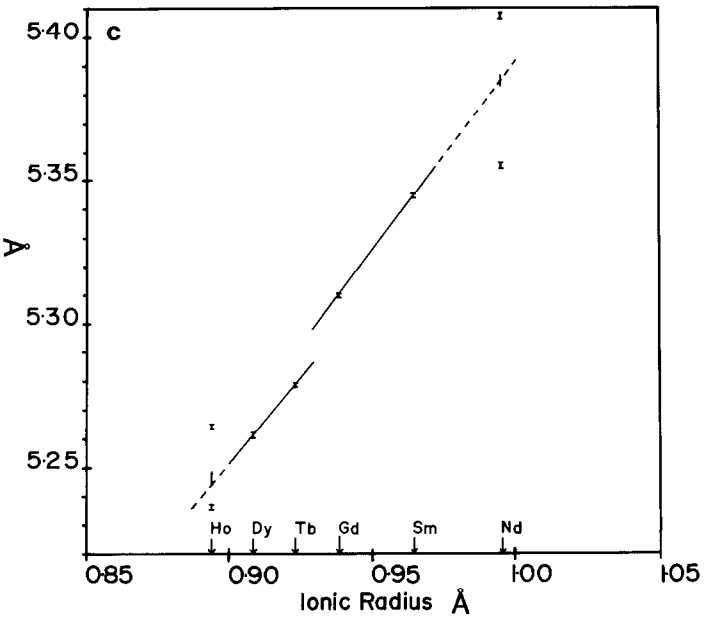

FIG. 1—*Continued*

have attempted to extract reliable information as to the type and extent of such compositional and displacive modulation from diffraction data (*5–10*). To date, however, the results have tended to be somewhat confusing if not mutually contradictory. Thus, for example, Steele and Fender (*6*) and Morinaga *et al.* (*8*) agree that oxygen ions in the ~20–30 mole% $YO_{1.5}$ in ZrO_2 "C_1" solid solution region are displaced ~0.25 Å along ⟨100⟩ directions, whereas Horiuchi *et al.* (*9*) did not find a significant proportion of oxygen ions displaced along ⟨100⟩. Due to the difficulty of accurate measurement and subsequent interpretation, diffuse intensity distributions have been somewhat neglected in favor of the (at least potentially) refinable, fluorite-related superstructure phases which can sometimes be obtained via prolonged annealing at lower temperatures (*11, 12*). The natural tendency has been to interpret the diffuse intensity distributions of the high temperature solid solution phases in terms of small microdomains of the lower temperature ordered phases (*8, 13*).

Increasing further the proportion of the lower valent metal oxides apparently leads to the stabilization of structure types not found in the pure ZrO_2 (although still closely related to the cubic fluorite-type parent phase and describable as compositional and displacively modulated variants thereof) such as the pyrochlore and C-type solid solution fields commonly reported at high temperatures (>1600°C) in ZrO_2–Ln_2O_3 systems (*14*). A typical phase diagram of these anion-deficient phases at high temperatures (~1600°C) and as a function of increasing Ln_2O_3 concentration (*14*) shows an initial tetragonal solid solution region giving way first to a cubic fluorite-related solid solution region which in turn gives way either to a pyrochlore region and thence to a C-type solid solution field or directly to the C-type region depending upon the particular lanthanide. In the case of the lighter rare earth

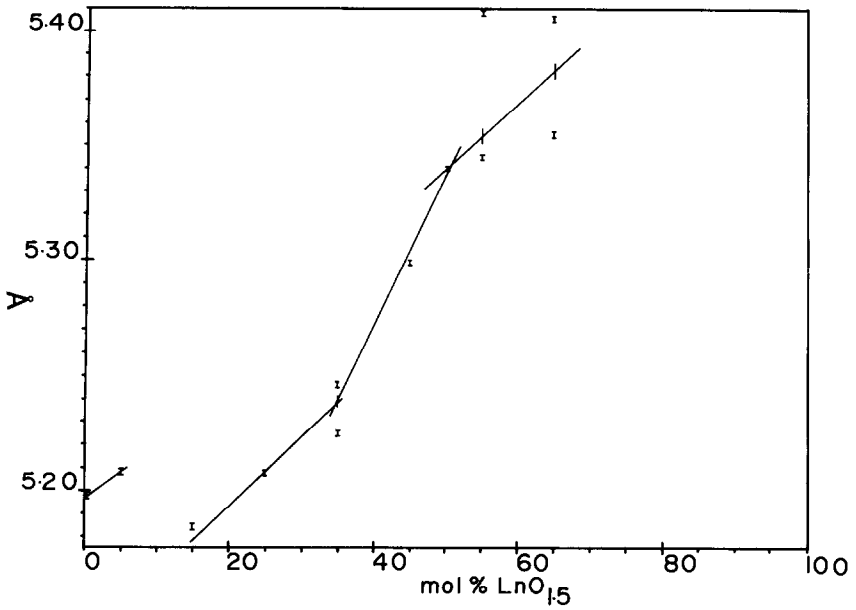

FIG. 2. Plot of the cubic unit cell dimension as a function of composition for the ZrO_2–$NdO_{1.5}$ system. For the monoclinic region (0–5 mol%), the cube root of the unit cell volume was used while for the pyrochlore region half the cell edge was used.

elements, increasing still further the proportion of the lower valent metal oxides leads to the stabilization of structure types not related to the cubic fluorite-type parent phase (and hence not the preserve of this paper) such as, for example, the A-type and B-type sesquioxide structures.

Despite much attention, many questions still remain: first, whether there are, of necessity, diphasic regions separating these various fluorite-related, cubic solid solution fields (*14–16*); second, if there are such diphasic regions, then what is the nature of the structural difference between the various solid solution fields; and, third, what is the nature of the structural variation within or across such solid solution fields (*17*). In a recent TEM study of a closely related system (CeO_2–Y_2O_3) it became clear, first, that the reported F-type solid solution region contained extra satellite reflections in addition to the sharp bragg reflections of the average cubic fluorite-type structure and, hence, should not be labeled F-type at all and, second, that the structural difference between the F- and C-type solid solution regions within this system is rather more subtle than had hitherto been supposed (*18, 19*). The purpose of this paper is to present the results of a combined X-ray powder, and electron, diffraction study of the compositional and displacive ordering present in the fluorite-related cubic phases of ZrO_2–Ln_2O_3 systems (typically quenched from temperatures ~1600°C) and to use these results to provide insight into the above questions.

2. Experimental

A selection of ZrO_2 : $LnO_{1.5}$ specimens were prepared to address the questions raised above. In the system ZrO_2 : $NdO_{1.5}$, which is reported at 1600°C to display significant solid solution fields of so-called

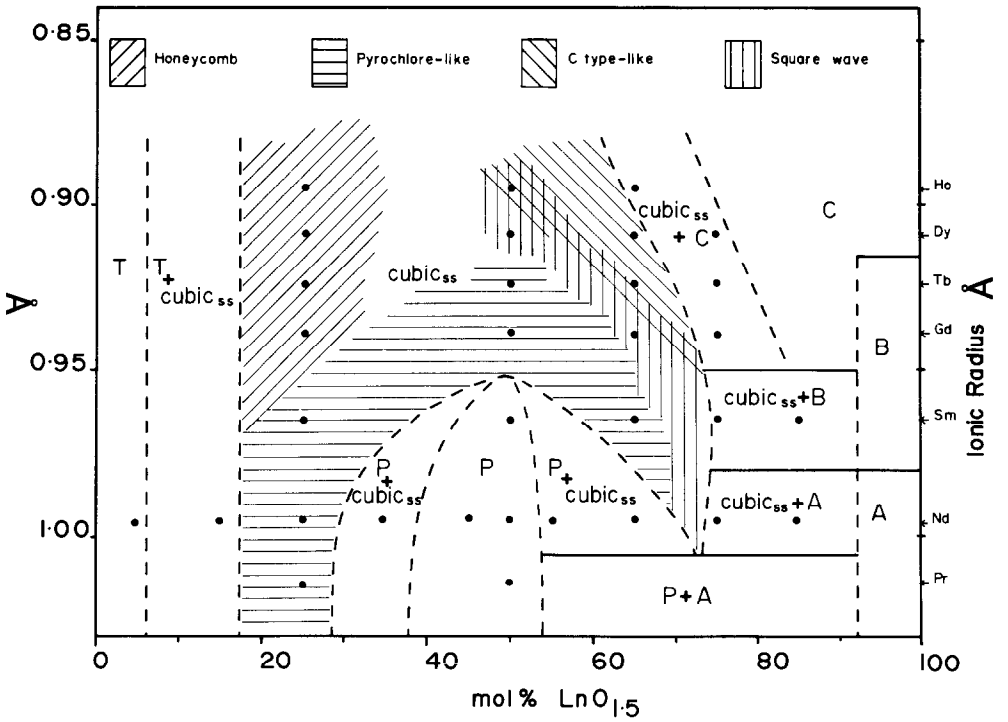

FIG. 3. Summary of the phase relationships of the system ZrO_2–$LnO_{1.5}$ quenched from 1600°C under oxidizing conditions, as a function of lanthanide ionic radius (similar to Fig. 27.2 in Ref. (*20*)). Data points are represented by filled circles. The solid solution, $cubic_{ss}$, is described as a single phase but has been subdivided into regions according to the type of diffuse intensity distribution observed via electron diffraction.

"C_1" (fluorite) type, pyrochlore type, and "C_2" (Tl_2O_3) type, specimens were prepared at 5, 15, 25, 35, 45, 50, 55, 65, 75, and 85 mole% $NdO_{1.5}$ in ZrO_2. In addition, specimens of the other light rare earth elements (Pr, Sm, Gd, Tb, Dy, and Ho) were also prepared at 25 mole% $LnO_{1.5}$ in ZrO_2 in their C_1 fields, at 50 mole% in their pyrochlore or C_1 fields, and at 65 mole% (Sm, Gd, Tb, Dy, and Ho) and 75 mole% (Sm, Gd, Tb, and Dy) within or containing the end member of their C_2 fields.

Starting materials (Research 99.9% for lanthanide oxides, Z-Tech >99.9% "ZrO_2" (2.57% HfO_2)) were fired at 1000°C before weighing. The component oxides were thoroughly mixed mechanically before being pressed into pellets. The pellets were placed on alumina tiles and heated at 1600°C for ~5 days then remixed and repelleted before heating again at 1600°C for 2–3 days. Platinum support and vessels were avoided due to the reaction of platinum with the lighter rare earth containing specimens. Typically specimens were quenched in water from 1600°C, though Nd containing specimens and the 25 mole% $HoO_{1.5}$ in ZrO_2 specimen were also cooled in the furnace to 1000°C before air-quenching to observe the effects of quench rate on structure and phase relationships. The course of reaction was monitored at each step by XRD using a Guinier–Hägg camera with monochromated Cu$K\alpha_1$ radiation. The attainment of equilib-

rium was determined by the observation of a single set of, or in the case of specimens in two phase regions two sets of, sharp diffraction lines extending to high angle. For the heavier of the lanthanides it was sometimes necessary to add an additional cycle to the synthesis procedure described above in order to meet this criterion. It was notable that for a given specimen the observed characteristic diffuse distribution was virtually insensitive to whether or not the specimen had attained equilibrium according to our XRD-based criterion.

For the determination of the unit cell dimensions by least squares refinement an internal standard of Si (NBS No. 640) was added to calibrate the measurement of XRD films. For the recording of electron diffraction patterns specimens were crushed, dispersed onto 3-mm holey carbon-coated copper grids and examined in a JEOL 100CX transmission electron microscope.

3. Results and Discussion

3.1 X-Ray Powder Diffraction

The rate of reaction of the specimens decreased with increasing atomic number of the lanthanide. This can be understood in terms of proximity to the liquidus as defined previously (*14*). The refined unit cell dimensions are shown in Figs. 1 and 2 for the series of compounds studied. Figure 1 shows the refined unit cell dimensions as a function of ionic radius for (a) the 25 mole% (b) the 50 mole%, and (c) the 65 mole% $LnO_{1.5}$ specimens. As expected, there is an increase in the cubic unit cell dimension with increasing ionic radius. However, there are noticeable deviations from linearity in both the 25 and the 65 mole% $LnO_{1.5}$ series. In the 65 mole% case, the points for Nd and Ho have been interpolated from the weighted average unit cell dimensions derived from the two cubic phases observed at this composition. The weighting was calculated from the relative intensities of equivalent reflections in the powder diffraction patterns. The 50 mole% $LnO_{1.5}$ case was approximately linear though it gives a less satisfactory fit than the 25 mole% case, which also only contained one cubic phase at equilibrium.

Figure 2 shows a plot of the cubic unit cell dimension as a function of composition for the ZrO_2–$NdO_{1.5}$ system. For the monoclinic region (0–5 mole%), the cube root of the unit cell volume was used while for the pyrochlore region half the cell edge was used. As for Fig. 1c, the weighted average cubic cell edge was used in the two phase regions. Notably, the slope of the lines is approximately the same for all compositions except for the pyrochlore solid solution region. Also evident is the quasivolume increase observed when transforming from the cubic zirconia structure to the baddeleyite structure.

In Fig. 3 we have attempted to summarize the phase relationships of the system ZrO_2–$LnO_{1.5}$ at 1600°C in air, as a function of ionic radius (similar to Fig. 27.2 in Ref. (*20*)). The detail in this figure somewhat anticipates the observed electron diffraction

FIG. 4. Typical small condensor aperture ⟨110⟩ zone axis CBPs for 25 mole% (a) Pr, (c) Nd, (d) Sm, (e) Gd, (f) Tb, (g) Dy, and (h) Ho $LnO_{1.5}$ in ZrO_2 specimens. In the case of Nd specimens quenched from within the diphasic regions ($cubic_{ss}$ + T and $cubic_{ss}$ + P) bounding the $cubic_{ss}$ solid solution region (i.e., at 15 and 35 mole%), some variability in the "C_1" diffraction patterns obtained was observed. Usually the ⟨110⟩ CBP shown in (c) was obtained but occasionally that shown in (b) was found. In each case the strongest reflections correspond to the underlying fluorite-related average structure. The first strong reflection in the horizontal direction is the {002}* and the first strong reflection in the vertical direction is the {220}*.

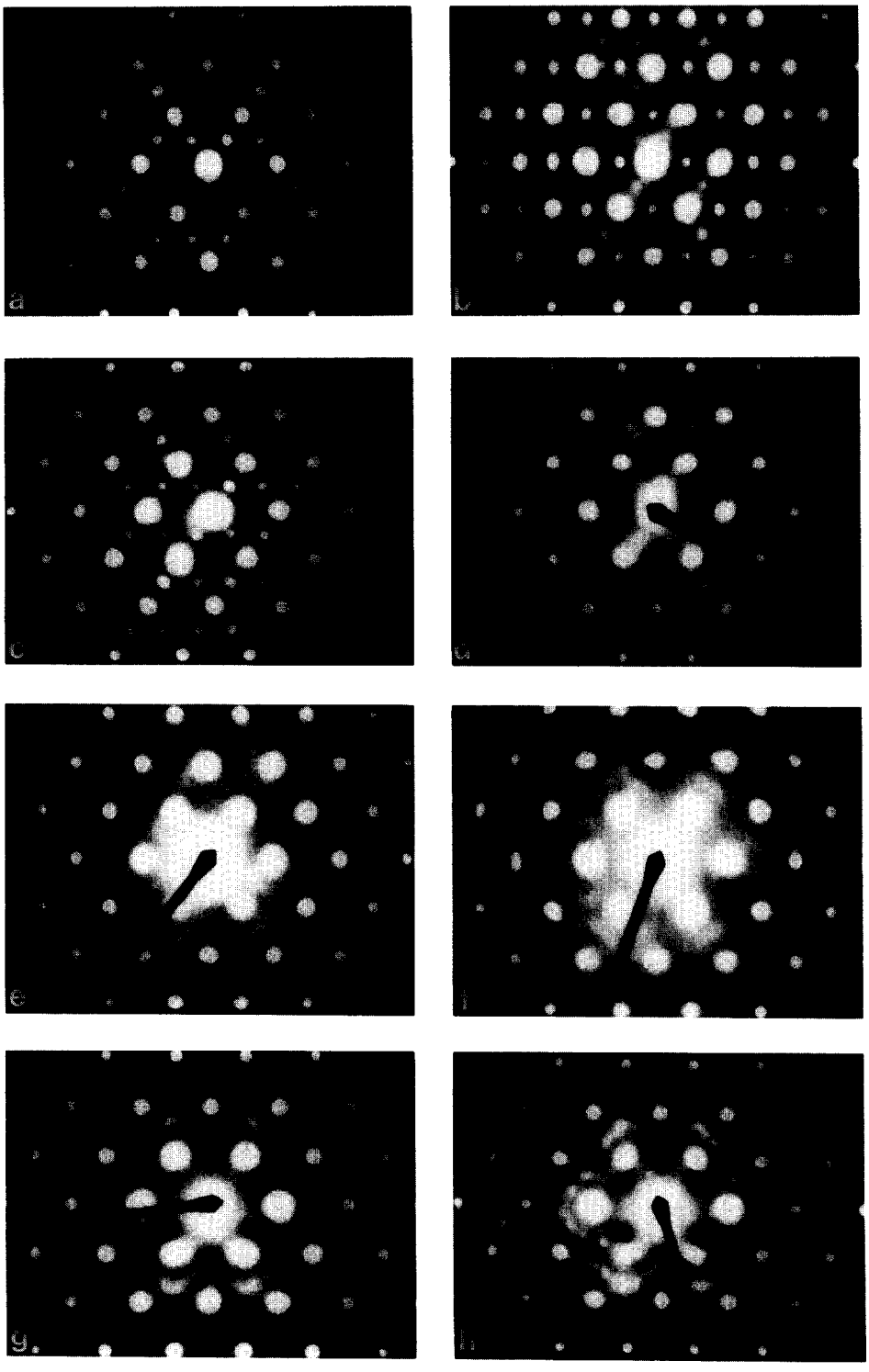
a
b
c
d
e
f
g
h

results which are to be discussed below. However, the major feature of this quasiphase diagram is the treatment of the phases formerly labeled as C_1 and C_2 as a continuous single solid solution region labeled $cubic_{ss}$. Specimens at the edge of solid solution regions which were not quenched from 1600°C tend to show some unmixing.

3.2 Electron Diffraction

Selected area electron diffraction patterns (SADPs) and convergent beam electron diffraction patterns (CBPs) were obtained for all samples along all major zone axes. Diffraction patterns obtained from different grains within the same preparation were almost always internally self-consistent and reproducible. In every case there is a set of strong, sharp Bragg reflections (the matrix reflections) consistent with an underlying, fluorite-type (*Fm3m*) average structure and labeled $\mathbf{G_F}$ in what follows. In addition, however, there are usually sets of weaker, but still sharp, satellite reflections (at $\mathbf{G_F} \pm \mathbf{q}$) surrounding the matrix reflections—as well as characteristic diffuse intensity distributions. In the case of the C-type structure, two sets of satellite reflections should be observed—namely the $\mathbf{G_F} \pm \frac{1}{4}\{220\}^*$ and $\mathbf{G_F} \pm \{001\}^*$ type satellite reflections. In the case of the pyrochlore structure, two sets of satellite reflections should also be observed—namely the $\mathbf{G_F} \pm \frac{1}{2}\{111\}^*$ and $\mathbf{G_F} \pm \{001\}^*$ type satellite reflections. ⟨110⟩ zone axis diffraction patterns are invariably the most informative as all of the above types of satellite reflections can be observed simultaneously. To avoid confusion, all diffraction patterns are indexed with respect to the parent cubic fluorite cell.

3.2.1 *⟨110⟩ Zone Axis Diffraction Patterns Characteristic of 25 mole% $LnO_{1.5}$*

Figure 4 shows typical small condensor aperture ⟨110⟩ zone axis CBPs for 25 mole% (a) Pr, (c) Nd, (d) Sm, (e) Gd, (f) Tb, (g) Dy, and (h) Ho $LnO_{1.5}$ specimens, i.e., within the previously labeled C_1, or cubic fluorite-type, solid solution field (*14*) (Such small condensor aperture CBPs tend to show up the existence of weak diffuse intensity distributions better than the corresponding selected area diffraction patterns). The Pr C_1 specimen, however, shows quite sharp $\mathbf{G_F} \pm \frac{1}{2}\{111\}^*$ type satellite reflections in addition to the fluorite-type average structure reflections as well as weak diffuse streaking along the $\{111\}^*$ directions of reciprocal space. The Nd specimen similarly shows quite sharp (although not as sharp as for the Pr C_1 specimen) $\mathbf{G_F} \pm \frac{1}{2}\{111\}^*$ type satellite reflections as well as the beginnings of a characteristic honeycombed diffuse intensity distribution which develops ever more strongly through the Sm, Gd, Tb, Dy, and Ho specimens. (In the case of the Nd specimens quenched from within the diphasic regions ($cubic_{ss}$ + T and $cubic_{ss}$ + P) bounding the $cubic_{ss}$ solid region (the 15 and 35 mole% specimens), some variability in the C_1 diffraction patterns obtained was observed. Usually the ⟨110⟩ CBP shown in Fig. 4c was obtained but occasionally that shown in Fig. 4b was found. When quenched from within the $cubic_{ss}$ solid solution field, however, the CBP shown in Fig. 4c was always

FIG. 5. Small condensor aperture ⟨110⟩ zone axis CBPs for the 50 mole% (a) Pr, (b) Sm, (c) Gd, (e) Tb, (g) Dy, and (h) Ho $LnO_{1.5}$ in ZrO_2 specimens. The SADPs corresponding to the Gd and Tb specimens are shown in (d) and (f), respectively. In each case the strongest reflections correspond to the underlying fluorite-related average structure. The first strong reflection in the horizontal direction is the $\{002\}^*$ and the first strong reflection in the vertical direction is the $\{220\}^*$.

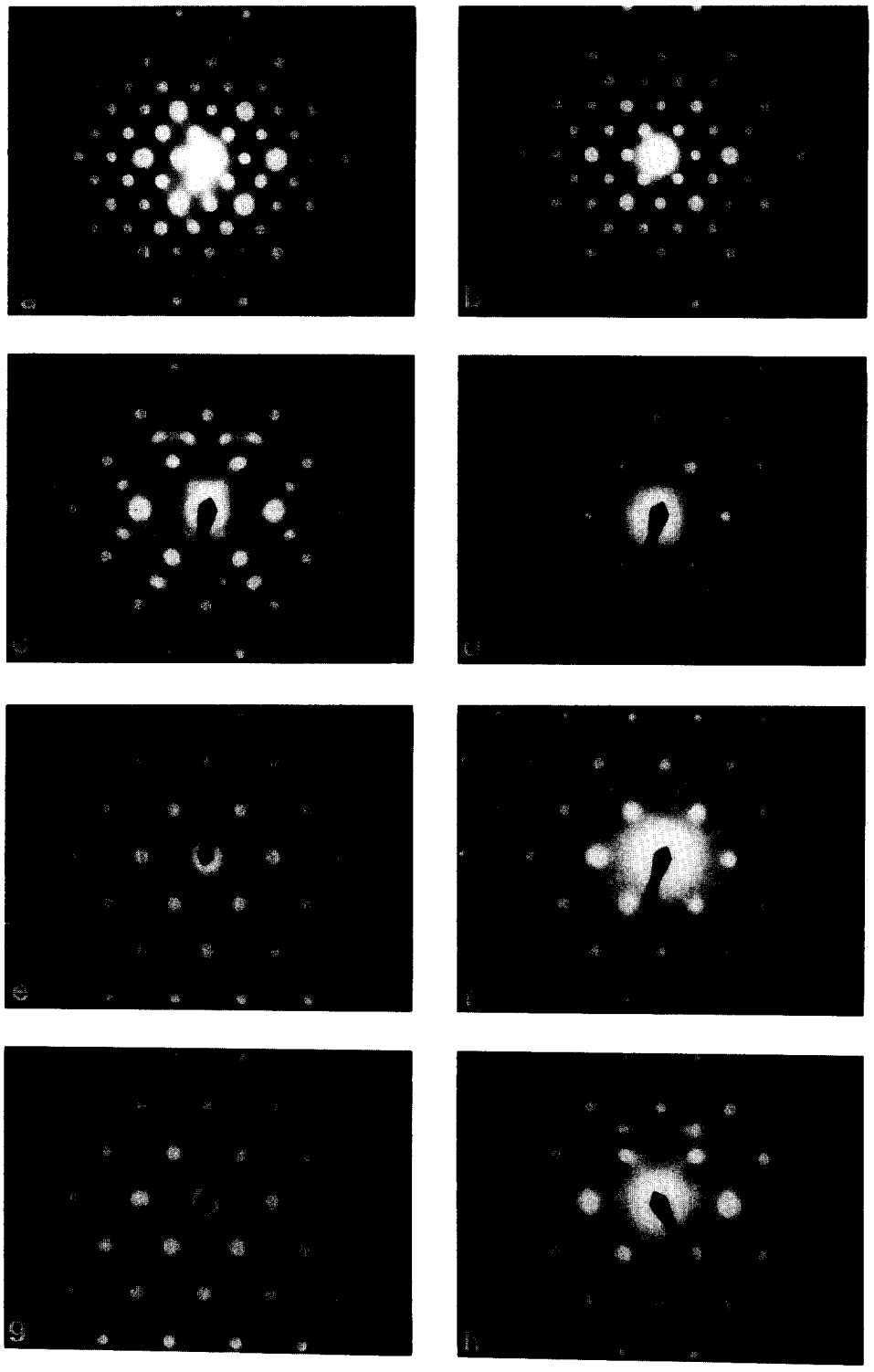

obtained.) The Pr and Nd C_1 specimens would therefore appear to be pyrochlore-, rather than fluorite-, related. Note, however, that the expected $\mathbf{G_F} \pm \{001\}^*$ satellite reflections of the pyrochlore structure type are very weak if not totally absent. This situation is very reminiscent of what was found in the so-called F-type solid solution region of the CeO_2–Y_2O_3 system, i.e., the $\mathbf{G_F} \pm \frac{1}{4}\{220\}^*$ satellite reflections characteristic of the C-type solid solution region were found but the $\mathbf{G_F} \pm \{001\}^*$ satellite reflections also characteristic of the C-type solid region appeared to be absent. The Sm specimen shows diffuse blobs in the same regions of reciprocal space (i.e., at $\mathbf{G_F} \pm \frac{1}{2}\{111\}^*$) as well as a more developed characteristic honeycomb diffuse intensity distribution which develops ever more strongly through the Gd, Tb, Dy, and Ho specimens. In these latter specimens, the only Bragg reflections observed correspond to the underlying fluorite-related average structure and, hence, the phases could be labeled cubic fluorite-like, or F-type, although it is unclear, given the more-or-less smooth variation in diffraction patterns observed in moving from the Pr to the Ho specimen, whether such labeling schemes (based solely upon the observed sharp Bragg reflections) are very useful. In any event, the anion vacancies and presumably also the metal atoms are not randomly distributed, otherwise the diffuse intensity distribution would not have the characteristic honeycomb pattern experimentally observed. Note the similarity of this diffuse intensity distribution to that recently reported for ~33 mole% $YO_{1.5}$ in ZrO_2 (*10*).

3.2.2 ⟨*110*⟩ *Zone Axis Diffraction Patterns Characteristic of 50 mole% $LnO_{1.5}$*

Figure 5 shows corresponding small condensor aperture ⟨110⟩ zone axis CBPs for the 50 mole% (a) Pr, (b) Sm, (c) Gd, (e) Tb, (g) Dy and (h) Ho $LnO_{1.5}$ specimens. The Pr, Nd, and Sm specimens are all within their pyrochlore solid solution fields and show the characteristically sharp $\mathbf{G_F} \pm \frac{1}{2}\{111\}^*$ and $\mathbf{G_F} \pm \{001\}^*$ type satellite reflections. Comparison with the 25 mole% Pr and Nd C_1 ⟨110⟩ zone axis CBPs (see Figs. 4a and 4c) shows the partial nature of the pyrochlore type ordering of the latter specimens. The Gd and Tb CBPs show diffuse blobs, rather than sharp satellite reflections, in the vicinity of the $\mathbf{G_F} \pm \frac{1}{2}\{111\}^*$ regions of reciprocal space. Furthermore, intensity has disappeared altogether from the $\mathbf{G_F} \pm \{001\}^*$ regions of reciprocal space. The corresponding selected area diffraction pattern (SADP) for the Gd specimen (d) shows the presence of localized diffuse streaking perpendicular to the $\{111\}^*$ directions of reciprocal space (but running through the $\mathbf{G_F} \pm \frac{1}{2}\{111\}^*$ positions). In the case of the Tb specimen (f) the corresponding SADP shows that the diffuse streaking present in the CBP is due to two apparently sharp satellite reflections on either side of the $\mathbf{G_F} \pm \frac{1}{2}\{111\}^*$ positions of reciprocal space. Detailed tilting experiments, however, show that these are not incommensurate satellite reflections but rather constitute part of a circle of diffuse

FIG. 6. Corresponding small condensor aperture ⟨110⟩ zone axis CBPs for the 65 mole% (c) Sm, (d) Gd, (e) Tb, (f) Dy, and (g) Ho $LnO_{1.5}$ in ZrO_2 specimens. The 65 mole% $NdO_{1.5}$ specimen was in the two phase pyrochlore plus $cubic_{ss}$ region. The ⟨110⟩ zone axis CBP characteristic of the ~55 mole% Nd pyrochlore solid solution field is shown in (a) while that characteristic of the ~70 mole% Nd $cubic_{ss}$ specimen is shown in (b). In each case the strongest reflections correspond to the underlying fluorite-related average structure. The first strong reflection in the horizontal direction is the $\{002\}^*$ and the first strong reflection in the vertical direction is the $\{220\}^*$.

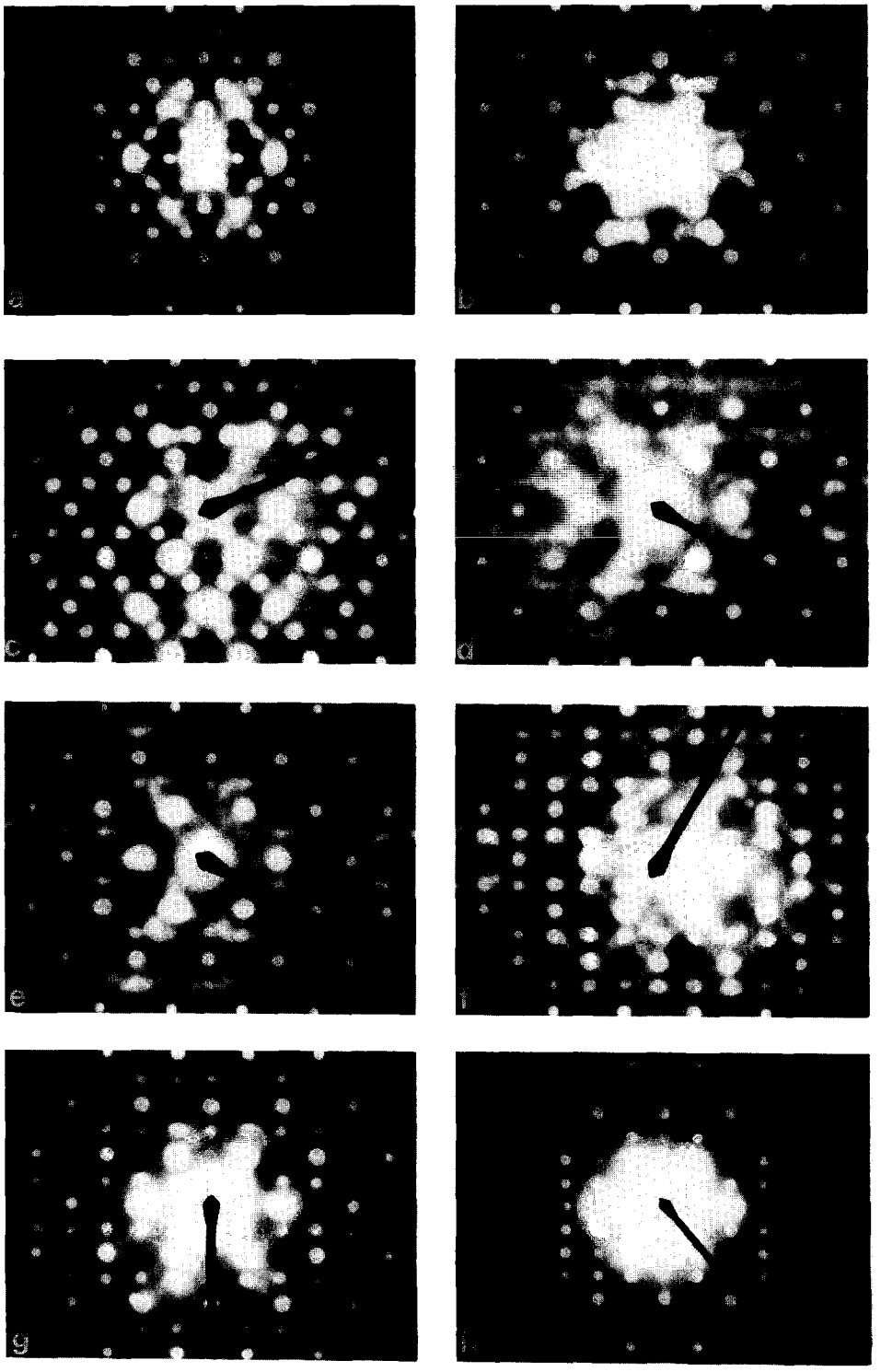
a
b
c
d
e
f
g
h

intensity. In the case of the Dy specimen, the localized diffuse blobs in the vicinity of the $\mathbf{G}_F \pm \frac{1}{2}\{111\}^*$ regions of reciprocal space have blurred out into a more continuous square wave type of diffuse intensity distribution running very roughly along the $\{001\}^*$ directions of reciprocal space. This continuous distribution runs through both the $\mathbf{G}_F \pm \frac{1}{2}\{111\}^*$ and the $\mathbf{G}_F \pm \frac{1}{4}\{220\}^*$ regions of reciprocal space. Finally, in the case of the Ho specimen, the diffuse distribution now appears to be more localized in the vicinity of the $\mathbf{G}_F \pm \frac{1}{4}\{220\}^*$ rather than the $\mathbf{G}_F \pm \frac{1}{2}\{111\}^*$ region of reciprocal space. Thus, at least as far as the diffuse intensity distributions are concerned, there would appear to be a more or less smooth transition from pyrochlore-related to C-type-related as a function of the lanthanide for the 50 mole% $Ln\mathrm{O}_{1.5}$ specimens. Figure 1b shows the cubic fluorite cell edge for each of these 50 mole% $Ln\mathrm{O}_{1.5}$ specimens as a function of the ionic radius of the lanthanide with a surprisingly linear relationship.

3.2.3 *⟨110⟩ Zone Axis Diffraction Patterns Characteristic of 65 mole% $Ln\mathrm{O}_{1.5}$*

Figure 6 shows the corresponding small condensor aperture ⟨110⟩ zone axis CBPs for the 65 mole% $Ln\mathrm{O}_{1.5}$ specimens, i.e., generally within the previously labeled C_2 or C-type cubic solid solution field (*14*). The 65 mole% $\mathrm{NdO}_{1.5}$ specimen was in the two-phase pyrochlore plus cubic_{ss} region. Thus the ⟨110⟩ zone axis CBP characteristic of the Nd pyrochlore solid solution field is also shown (Fig. 6a). The Nd cubic_{ss} specimen (b) shows a very strong and characteristic diffuse distribution running approximately along the $\{001\}^*$ directions of reciprocal space and almost taking the form of a square wave. It is very similar to the square wave type of diffuse distribution observed for the 50 mole% Dy specimen (see Fig. 5g). The intensity in the diffuse distribution appears to be fairly evenly distributed and again runs through both the $\mathbf{G}_F \pm \frac{1}{2}\{111\}^*$ and the $\mathbf{G}_F \pm \frac{1}{4}\{220\}^*$ positions of reciprocal space. Thus there is certainly no reason for this phase to be labelled C-type. The Sm specimen (c) shows a diffuse distribution in which intensity appears to have concentrated into diffuse blobs in the region of the $\mathbf{G}_F \pm \frac{1}{2}\{111\}^*$ positions of reciprocal space, i.e., more pyrochlore-related. Indeed the 65 mole% Sm CBP closely resembles the Pr and Nd C_1 CBPs (see Figs. 4a and 4c; there would appear to be a halo of such a pyrochlore-related phase surrounding the cubic_{ss}-P phase boundary in the quasiphase diagram of Fig. 3). The diffuse blobs at $\mathbf{G}_F \pm \frac{1}{2}\{111\}^*$ have blurred back into a square wave type of distribution for the Gd specimen (d). In the case of the Tb specimen (e) diffuse blobs in the vicinity of the $\mathbf{G}_F \pm \frac{1}{4}\{220\}^*$ positions of reciprocal space (characteristic of the C-type structure) have become noticeable although a diffuse distribution is still strongly visible. The diffuse blobs at $\mathbf{G}_F \pm \frac{1}{4}\{220\}^*$ have sharpened considerably in the Dy specimen (f) while the shape of the accompanying diffuse distribution has changed significantly to a more sinusoidal shape. The Ho specimen was in the diphasic region separating the cubic_{ss} and C-type solid solution fields (previously reported as the cubic fluorite (Ho F-type) and C-type (Ho C-type) solid solution fields). The diffuse distribution in the Ho cubic_{ss} CBP (g) has now virtually disappeared and we are left with sharp satellite reflections at the $\mathbf{G}_F \pm (\frac{1}{4} + \delta)\{220\}^*$ positions of reciprocal space. Notice that $\delta \neq 0$, i.e., it is incommensurately modulated (the same phenomenon was reported for 57 mole% $\mathrm{YO}_{1.5}$ in ZrO_2 (*10*)). Notice also the total absence of second harmonic $\mathbf{G}_F \pm \{001\}^*$ type satellite reflections. Thus, as for the analogous transition in the CeO_2–$\mathrm{Y}_2\mathrm{O}_3$ system (*19*), the two-phase region can be put down to the sudden onset of compositional and/or displacive modulation associated with the second harmonic $\mathbf{q} = \{001\}^*$ modulations. Finally, the Ho C-type CBP (h) is characteristic of the C-type structure exhib-

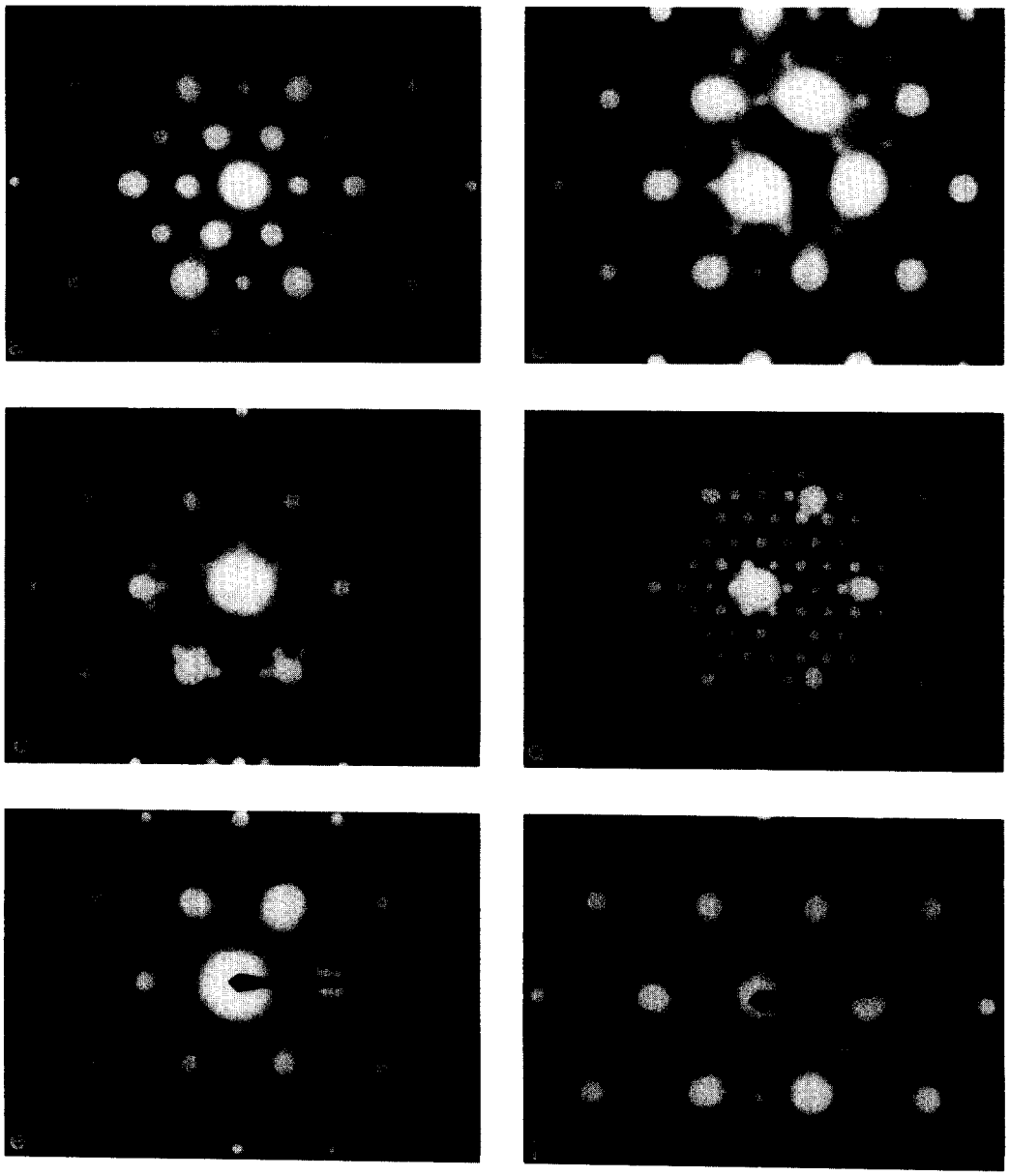

FIG. 7. The ⟨111⟩ zone axis CBPs characteristic of the Nd pyrochlore phase (a), the 25 mole% Pr "C_1" phase (b), the end member Ho-rich cubic$_{ss}$ phase (c), the end member Ho-poor, or C-type, phase (d), the 25 mole% Ho cubic$_{ss}$ phase (e), and the Nd specimen corresponding to Fig. 4b, (f). In each case the strongest reflections correspond to the underlying fluorite-related average structure. The first strong reflection in the horizontal direction is the {220}*.

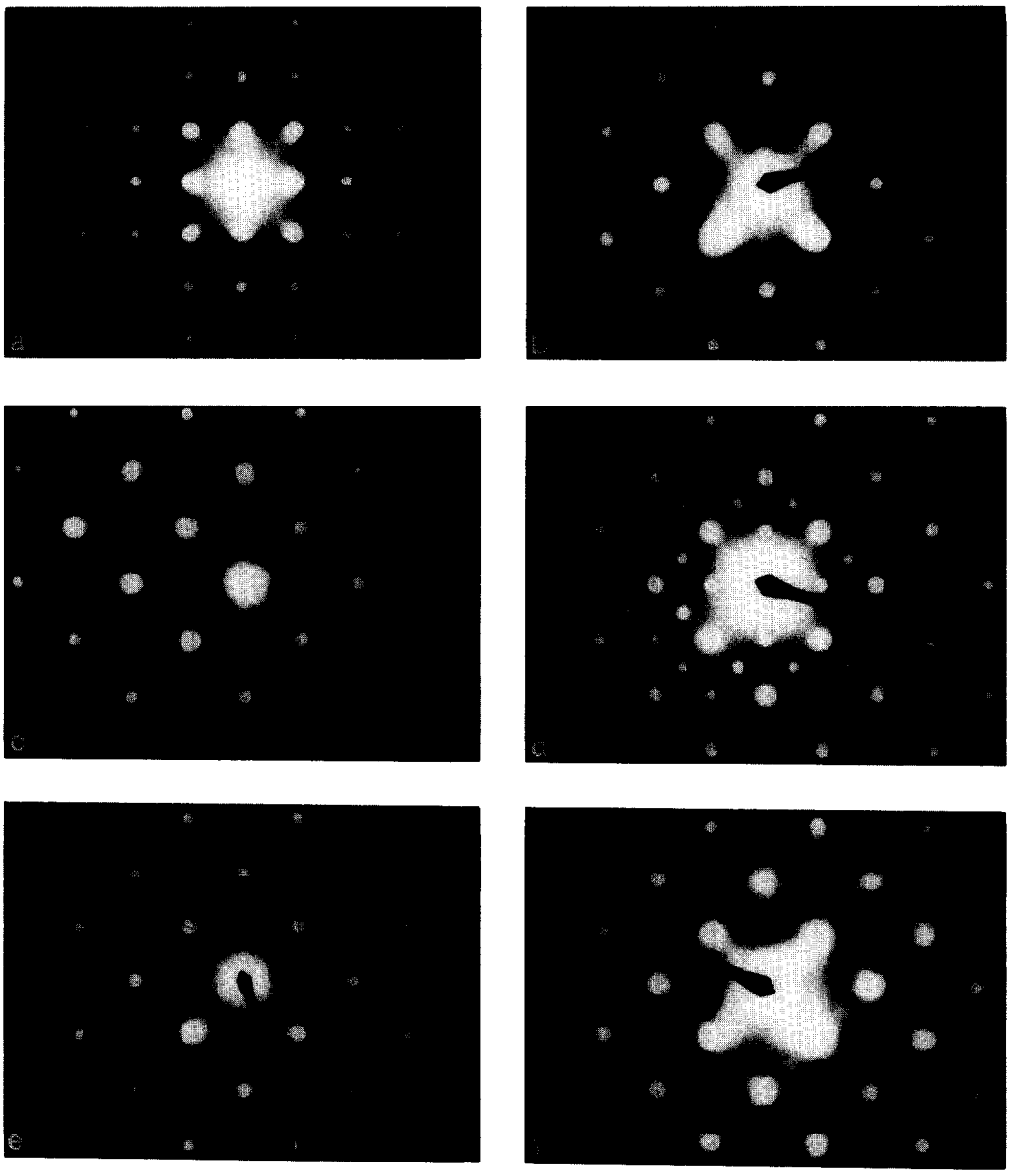

FIG. 8. The ⟨001⟩ zone axis CBPs characteristic of the Nd pyrochlore phase (a), the 65 mole% Sm $cubic_{ss}$ phase (b), the 65 mole% Dy $cubic_{ss}$ phase (c), the 75 mole% Gd C-type phase (d), the 25 mole% Dy $cubic_{ss}$ phase (e), and the Nd specimen corresponding to Fig. 4b, (f). In general, there is always very little diffuse scattering observed at ⟨001⟩ zone axes. In each case the strongest reflections correspond to the underlying fluorite-related average structure. The first strong reflection in the horizontal direction is the $\{2,-2,0\}^*$ and the first strong reflection in the vertical direction is the $\{220\}^*$.

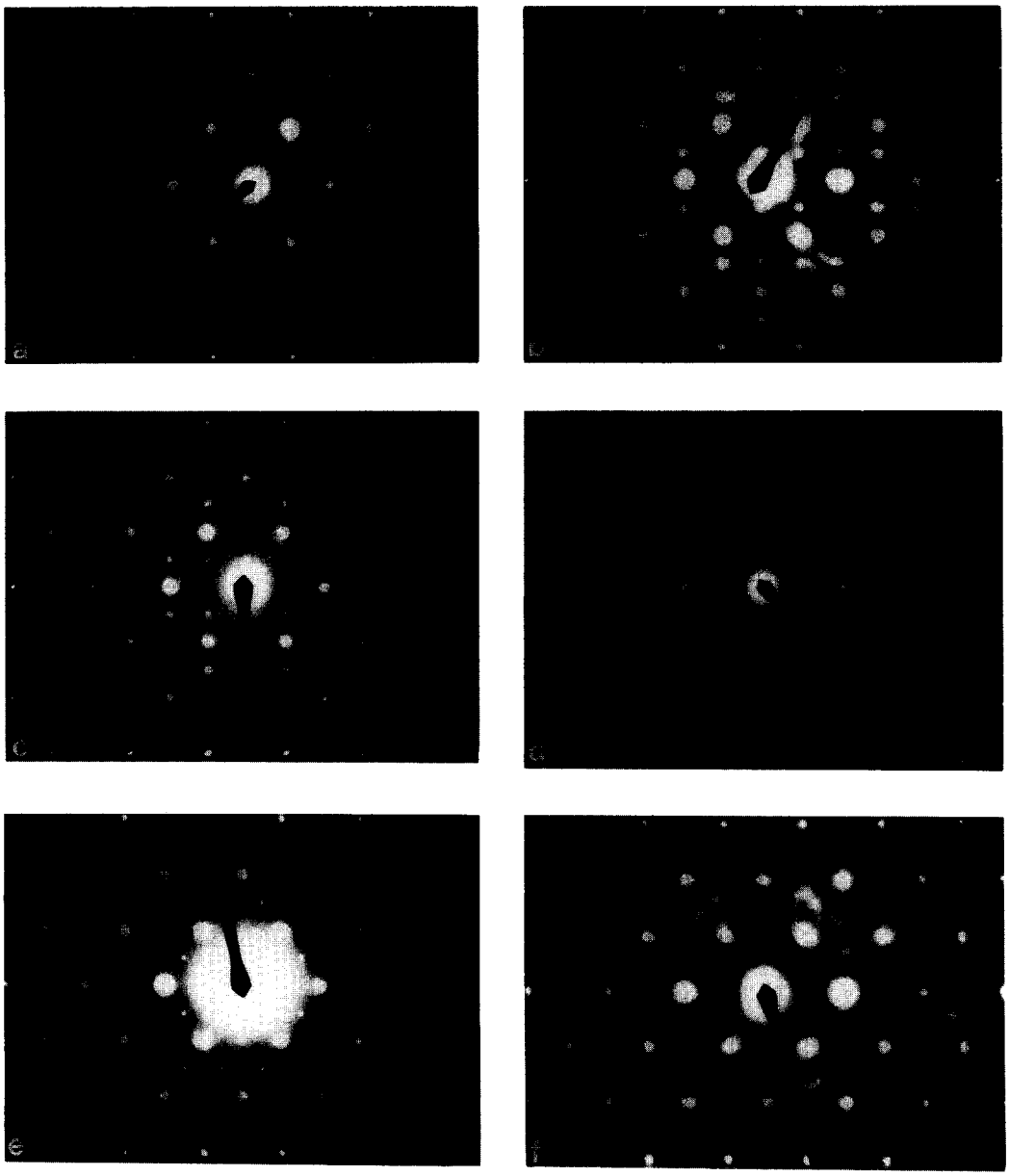

FIG. 9. The ⟨110⟩ zone axis SADPs of (a) the 65 mole% Nd $cubic_{ss}$, (b) the 65 mole% Dy $cubic_{ss}$, (c) the 65 mole% Ho $cubic_{ss}$, (d) the 65 mole% Ho C-type, (e) the 25 mole% Pr $cubic_{ss}$, and (f) the 25 mole% Ho $cubic_{ss}$ specimens. In each case the strongest reflections correspond to the underlying fluorite-related average structure. The first strong reflection in the horizontal direction is the {002}* and the first strong reflection in the vertical direction is the {220}*.

iting both the $\mathbf{G_F} \pm \frac{1}{4}\{220\}^*$ and the $\mathbf{G_F} \pm \{001\}^*$ type satellite reflections. Figure 1c shows the corresponding cubic fluorite cell edge for each of these 65 mole% $Ln O_{1.5}$ specimens as a function of the ionic radius of the lanthanide. For the Ho specimen, the larger cell parameter corresponds to the C-type structure while the lower cell parameter corresponds to the cubic_{ss} structure while for the Nd specimen the larger cell parameter corresponds to the cubic_{ss} structure and the lower to the pyrochlore-type structure. In both cases the dotted line is drawn through the point corresponding to the weighted mean cell average (based on the observed relative intensities of equivalent reflections for the two phases present).

3.2.4 *Other Zone Axis Diffraction Patterns*

Figure 7 shows ⟨111⟩ zone axis CBPs characteristic of the Nd pyrochlore phase (Fig. 7a), the 25 mole% Pr C_1 phase (Fig. 7b), the end member Ho-rich cubic_{ss} phase (Fig. 7c), the end member Ho-poor, or C-type, phase (Fig. 7d), the 25 mole% Ho cubic_{ss} phase (Fig. 7e) and the Nd specimen corresponding to Fig. 4b (Fig. 7f). Comparison of Fig. 7a with Fig. 7b confirms that the nature of the ordering in the Pr and Nd C_1 specimens, while pyrochlore-related, is by no means the same as that in pyrochlore itself. Similarly, comparison of Fig. 7c with Fig. 7d confirms that there is a sudden sharp increase in the relative intensity of the $\mathbf{G_F} \pm \{001\}^*$ satellite reflections relative to the $\mathbf{G_F} \pm \frac{1}{4}\{220\}^*$ satellite reflections across the Ho cubic_{ss} + C diphasic solid solution region just as occurs in the closely related CeO_2–Y_2O_3 system.

Figure 8 shows ⟨001⟩ zone axis CBPs characteristic of the Nd pyrochlore phase (Fig. 8a), the 65 mole% Sm cubic_{ss} phase (Fig. 8b), the 65 mole% Dy cubic_{ss} phase (Fig. 8c), the 75 mole% Gd C-type phase (Fig. 8d), the 25 mole% Dy cubic_{ss} phase (Fig. 8e), and the Nd specimen corresponding to Fig. 4b (Fig. 8f). In general, there is always very little diffuse scattering observed at ⟨001⟩ zone axes. Note the clear difference between pyrochlore and C-type ⟨001⟩ zone axis diffraction patterns.

Good quality SADPs, if sufficiently intense, give a better indication of the sharpness of satellite reflections or diffuse intensity distributions than the corresponding CBPs. Thus Fig. 9 shows ⟨110⟩ zone axis SADPs of the (a) 65 mole% Nd cubic_{ss}, (b) the 65 mole% Dy cubic_{ss}, (c) the 65 mole% Ho cubic_{ss}, (d) the 65 mole% Ho C-type, (e) the 25 mole% Pr cubic_{ss}, and (f) the 25 mole% Ho cubic_{ss} specimens. Note the very characteristic diffuse intensity distributions of the 65 mole% Nd cubic_{ss} and the 25 mole% Ho cubic_{ss} specimens as well as the extremely sharp (and hence long range ordered) satellite reflections belonging to the 65 mole% Dy cubic_{ss}, the 65 mole% Ho cubic_{ss}, the 65 mole% Ho C-type, and the 25 mole% Pr cubic_{ss} specimens, respectively.

The pyrochlore solid solution field was found to extend from 38 to 55 mole% $NdO_{1.5}$ in ZrO_2 when quenched rapidly (in water) from 1600°C, which is a rather wider range of existence than that reported by Rouanet (*14*). However, slower cooling rates saw the rapid unmixing of the $NdO_{1.5}$-poor end member due to the narrowing of the solid-solution field with decreasing temperature. This interpretation was fully consistent with XRD data. No obvious differences, however, could be observed in diffraction patterns from specimens across this solid solution field.

4. Conclusions

An immediate consequence of a detailed electron diffraction study of the cubic, fluorite-related solid solution fields in ZrO_2–Ln_2O_3 systems is the realization that labels such as F-type (or C_1), C-type (or C_2), or pyrochlore as traditionally used are rather inappropriate and unhelpful when attempting to describe structural variations

across and between such solid solution fields. For example, it is clearly inappropriate to label the 25 mole% $PrO_{1.5}$ in ZrO_2 specimen as cubic fluorite-like (see Fig. 4a). The existence of sharp $\mathbf{G_F} \pm \frac{1}{2}\{111\}^*$ satellite reflections indicates a partial pyrochlore-type ordering. Whether this partial ordering involves the metal atoms, the oxygen vacancies, or both, however, will remain unclear unless a single-crystal X-ray structure refinement is carried out at this composition. Similarly it is inappropriate to label the reported Ho F-type solid solution field as cubic fluorite-like (see Fig. 6g). The existence of sharp $\mathbf{G_F} \pm (\frac{1}{4} + \delta)\{220\}^*$ satellite reflections indicates a close resemblance to the ideal C-type structure. In this case, however, we now have a good idea of the nature of the structural difference between the two solid solution fields (*19*) although confirmation would again require a single crystal X-ray diffraction study on either side of the observed two-phase region. For neither of the above examples, however, has the growth of single crystals been reported to date.

Clearly it is possible for there to be a much more gradual transition between apparently distinct structural types as a function of composition than was previously thought to be the case. While the variety of observed diffuse intensity distributions do not of themselves provide immediate answers to the nature of the oxygen vacancy clustering, metal atom ordering, etc., responsible, they do provide a crucial constraint on any proposed models for such real space modulation. The existence of such a rich variety of composition-dependent diffraction effects shows clearly that much still remains to be understood about ZrO_2–Ln_2O_3 systems.

References

1. G. TEUFER, *Acta Crystallogr. Sect. A* **15,** 1187 (1962).
2. K. NEGITA, *Acta Metall.* **37,** 313 (1989).
3. K. NEGITA AND H. TAKAO, *J. Phys. Chem. Solids* **50,** 325 (1989).
4. K. J. DE VRIES, T. VAN JIJK, AND A. J. BURGGRAAF, *in* "Fast Ion Transport in Solids" (Vashishta, Mundy, Shenoy, Eds.), Elsevier, North Holland (1979).
5. R. E. CARTER AND W. L. ROTH, *in* "Electromotive Force Measurements in High-Temperature Systems" (C. R. Alcock, Ed.), p. 125, The Institute of Mining and Metallurgy, Elsevier, New York (1968).
6. D. STEELE AND B. E. FENDER, *J. Phys. C. Solid State Phys.* **7,** 1 (1974).
7. J. FABER, M. H. MUELLER, AND B. R. COOPER, *Phys. Rev. B* **17,** 4884 (1978).
8. M. MORINAGA, J. B. COHEN, AND J. FABER, *Acta Crystallogr. Sect. A* **35,** 789 (1979).
9. H. HORIUCHI, A. J. SCHULTZ, P. C. W. LEUNG, AND J. M. WILLIAMS, *Acta Crystallogr. Sect. B* **40,** 367 (1984).
10. S. SUZUKI, M. TANAKA, AND M. ISHIGAME, *Jpn. J. Appl. Phys.* **24,** 401 (1985).
11. J. G. ALLPRESS, H. J. ROSSELL, AND H. G. SCOTT, *J. Solid State Chem.* **14,** 264 (1975).
12. H. J. ROSSELL AND H. G. SCOTT, *J. Phys. Colloq. C7* **38,** 7–28 (1977).
13. J. G. ALLPRESS AND H. G. SCOTT, *J. Solid State Chem.* **15,** 68 (1975).
14. A. ROUANET, *Rev. Int. Hautes Temp. Refract.* **8,** 161 (1971).
15. S. R. SKAGGS, Technical Report, Sandia Lab, Albuquerque, New Mexico, SC-RR-72-0031, p. 89 (1972).
16. D. J. M. BEVAN AND E. SUMMERVILLE, *in* "Handbook of the Physics and Chemistry of the Rare Earths" (Gscneider and L. Eyring, Eds.), Vol. 3, p. 401, North-Holland, (1979).
17. A. D. WADSLEY, *in* "Non-stoichiometric Compounds" (L. Mandelcorn, Ed.), p. 99 Academic Press, New York/London (1964).
18. R. WALLENBERG, R. WITHERS, D. J. M. BEVAN, J. G. THOMPSON, P. BARLOW, AND B. G. HYDE, *J. Less-Common Met.* **156,** 1 (1989).
19. R. L. WITHERS, R. WALLENBERG, D. J. M. BEVAN, J. G. THOMPSON, AND B. G. HYDE, *J. Less-Common Met.* **156,** 17 (1989).
20. L. EYRING, "Handbook of the Physics and Chemistry of the Rare Earths" (Gscneider and L. Eyring, Eds.), Vol. 3, p. 337, North-Holland Publishing Company (1979).